Dewetting Dynamics at a Polymer−Polymer Interface

S. Qu,[†] C. J. Clarke,[‡] Y. Liu,[†] M. H. Rafailovich,*[,†] J. Sokolov,[†] K. C. Phelan,[§] and G. Krausch[§]

Department of Materials Science and Engineering, State University of New York at Stony Brook, Stony Brook, New York 11794, Department of Chemistry, McGill University, 801 Sherbrooke Street West, Montreal, Quebec, H3A 2K6, Canada, and Fakultät für Physik, Universität Konstanz, Postfach 5560, 78434 Konstanz, Germany

Received August 30, 1996; Revised Manuscript Received March 12, 1997[⊗]

ABSTRACT: We have studied the dynamics of dewetting at the interface between polystyrene (PS) and poly(methyl methacrylate) (PMMA) as a function of the molecular weights of the two materials. Optical microscopy and atomic force microscopy have been used to follow the dewetting process and to image both the surface and interfacial structure in the vicinity of the growing holes. We determined the scaling behavior of the dewetting velocity as a function of the molecular weight of the dewetting species (PS). Different regimes are found depending on the PMMA molecular weight. For large PMMA molecular weights the dewetting velocity scales inversely with the PS viscosity, while for low PMMA molecular weights, the dewetting velocity is almost independent of the PS viscosity. The experimental data are in quantitative agreement with recent theoretical predictions.

Introduction

Wetting and dewetting of a surface by a liquid is a well-known phenomenon, which has been studied in various situations for some years. Recently, much attention has been focused on the wetting and dewetting behavior of thin polymer films.[1−6] The stability of polymer films against dewetting is of considerable technological interest because of their widespread use as coatings. In addition, thin polymer films with high molecular weights have proven to be ideal model systems for the study of wetting phenomena due to their low vapor pressure and due to the fact that their high viscosity facilitates the study of the dynamic behavior. While most studies on dewetting so far have dealt with thin liquid films on a solid substrate, the more complex situation of a liquid dewetting from a liquid substrate has received much less attention. Brochard-Wyart et al. recently presented a detailed theoretical study,[1] suggesting that liquid−liquid dewetting should exhibit a variety of different regimes depending mainly on the relative viscosities of the two liquids, the thicknesses of the respective liquid layers, and the surface and interfacial tensions involved. Martin et al.[5] reported experiments on the bursting of macroscopic liquid poly(dimethylsiloxane) (PDMS) films on (liquid) fluorinated PDMS lower layers. They observed a constant dewetting velocity, which depends on the viscosity of the substrate and decreases with increasing substrate viscosity. Recently, Lambooy and co-workers have reported a study of the dewetting of PS films on PMMA as a function of PMMA molecular weight.[6] They observed two regimes characterized by liquidlike lower layers (for low PMMA molecular weight) and solidlike substrates (for high PMMA molecular weight): at low PMMA molecular weights, the dewetting velocity decreased rapidly with increasing lower layer viscosity until it reached a minimum and, thereafter, increased slowly. (Throughout this paper we will refer to the PS as the upper layer, the PMMA as the lower layer, and the silicon wafer on which the films are supported as the substrate.) The authors were able to image the buried PS/PMMA interface around a growing hole with atomic force microscopy. They demonstrated that the dewetting velocity depends strongly on the amount of interface deformation between the two polymers, which itself is a function of the relative viscosities of the two materials.

While in the study by Lambooy and co-workers only qualitative comparison to Brochard-Wyart's theoretical work was possible, the present paper aims to test the theory in more detail and tries to establish a quantitative comparison between theory and experiment. We extended the study of dewetting at the PS/PMMA interface by systematic variation of the molecular weights (and hence the viscosities) of both the upper (PS) and lower (PMMA) layers.

We start with a brief review of the theory of dewetting on solid and liquid lower layers. Consider the system shown in Figure 1, where the A phase is a liquid and B is either a solid (Figure 1a) or a liquid (Figure 1b). The wetting behavior is described by the spreading parameter S:

$$S = \gamma_B - (\gamma_A + \gamma_{AB}) \tag{1}$$

γ_A and γ_B are the surface free energies (surface tensions) of A and B, respectively, and γ_{AB} is the A−B interfacial energy. A dewets B when $S < 0$. In this case there is a finite contact angle at the lines where air or vacuum and the A and B phases meet. For a solid lower layer at equilibrium, we obtain the familiar equation of Young,[7] by balancing the interfacial tensions (Figure 1a)

$$\cos \Theta_e = \left(\frac{\gamma_B - \gamma_{AB}}{\gamma_A} \right) \tag{2}$$

If the lower layer is a liquid, the AB interface is no longer constrained to be a plane, and A forms a lens to minimize the interfacial free energy (Figure 1b, the Neumann construction). Balancing the surface tensions horizontally and vertically in the limit of small angles leads to

$$S = -\frac{1}{2} \gamma \Theta_e^2 \tag{3}$$

where γ is an effective surface tension ($1/\gamma = 1/\gamma_A +$

[†] State University of New York at Stony Brook.
[‡] McGill University.
[§] Universität Konstanz.
[⊗] Abstract published in *Advance ACS Abstracts,* May 1, 1997.

S0024-9297(96)01297-1 CCC: $14.00

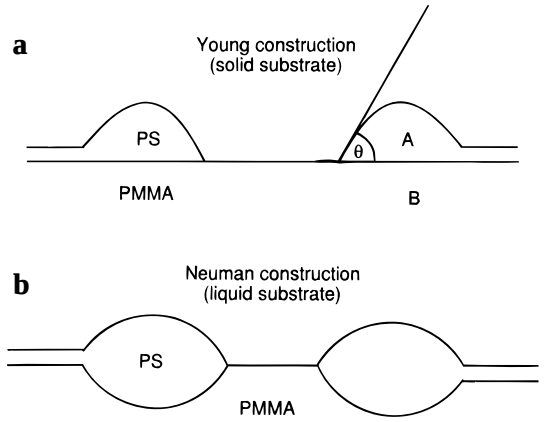

Figure 1. Schematic diagrams showing the hole and rim of part of a dewetting film: (a) solid lower layer; Young construction; (b) liquid lower layer, Neumann construction.

$1/\gamma_B$). The stability of a film with respect to dewetting is determined from the free energy per unit area. For macroscopic films (i.e., films thicker than a few micrometers), the free energy is given by a sum of capillary and gravitational energies, whereas for microscopically thin films, long-range van der Waals forces dominate.

So far we have only dealt with the equilibrium situation. We also wish to consider the dynamics of dewetting. According to the theoretical model,[1] dewetting is initiated by capillary waves, and it is the fastest growing mode which sets the length scale of the dewetting patterns. This has been experimentally verified recently, though heterogeneities in the film (e.g., dust particles) can also nucleate holes.[8] After a certain time, a dry patch appears in each trough of the capillary waves, thereby producing a cellular pattern of holes. Figure 1 shows schematically the early stage of dewetting on solid and liquid substrates, where a hole has formed in an unstable film. The hole is surrounded by a rim, which moves outward as dewetting proceeds. In the early stage of dewetting, a dynamic contact angle Θ_d is observed rather than the equilibrium contact angle Θ_e. When the holes have grown sufficiently large, the rims will meet and a transient two-dimensional foam is formed. The walls of the foam then break up into isolated droplets.[1−3]

Brochard-Wyart et al. have considered in detail the early stages of dewetting, i.e., the break up of the film and the formation and growth of holes. In the following, we will use the terminology of ref 1 for simplicity. Let η_i be the viscosities of the two liquid phases. Then, if $\eta_A << \eta_B$, the lower layer is solidlike. Two regimes are found in this case: a viscous regime (section C.a.1 in ref 1), where the liquid A is viscous and has a small contact angle, and an inertial regime (section C.a.2 in ref 1), where A has a low viscosity and a large contact angle. In the former case, the dewetting velocity is predicted to be constant (i.e., independent of time and hole diameter) and given by

$$v = \frac{1}{12 \ln \sqrt{2}} \frac{\gamma_A}{\eta_A} \Theta_e^{\,3} \tag{4}$$

Note that v is independent of the viscosity of the lower layer. Equation 4 is valid if the width of the rim (l) is smaller than the diameter of the hole (R), i.e., if the velocities of the inner and outer contact lines, which limit the rim, are the same. The velocities are related to the dynamic contact angle Θ_d, which in this regime is given by

$$\Theta_d = \Theta_e/\sqrt{2} \tag{5}$$

Conservation of the volume of A leads to a relation between the width of the rim and the diameter of the growing hole:

$$l(t) \propto \sqrt{R/\Theta_e} \tag{6}$$

Thus, since R increases linearly with time in the regime of constant dewetting velocity, $l \sim t^{1/2}$. The scaling of the dewetting velocity with the cube of the contact angle (eq 4) was first predicted by Tanner.[9] This regime has been studied in several systems, for example, macroscopic films of silicone oils and alkanes on solid substrate.[10] Reiter has studied the dewetting behavior of thin (microscopic) polymer films on solid substrates.[2] He found a constant dewetting velocity in agreement with the prediction of eq 4.

For the opposite case of a highly viscous liquid dewetting from a low-viscosity substrate

$$\frac{\eta_A}{\Theta_e} > \eta_B \tag{7}$$

viscous dissipation is dominated by the contribution of the lower layer. Here, three regimes are found: a viscous regime similar to the one discussed above (section C.b.1 in ref 1), a viscoinertial regime, where the penetration length of the flow into the lower layer induced by the motion of the rim is smaller than the rim size (section C.b.2 in ref 1), and a purely inertial regime (section C.b.3 in ref 1). The viscous regime can further be subdivided into two cases, depending on the thickness of the lower layer. In the case of a thick ("bulk") lower layer (section C.b.1ii), the dewetting velocity is given by

$$v = \frac{\gamma}{\eta_B} \Theta_e^{\,2} \tag{8}$$

Again, v is constant. In contrast to the situation described above, however, v now depends on the lower layer viscosity η_B rather than on η_A. For very thin lower films, or when the substrate is extremely smooth so that the polymer melt slips at the substrate surface, hole diameter grows as $t^{2/3}$ as given in eq 21, section C.b.1i of ref 1. By differentiating this, we find that the velocity is expected to decrease with time

$$v \propto \left(\frac{\eta_B^{\,2} L^2 \Theta_e}{\eta_B^{\,2} e} \right)^{1/3} t^{-1/3} \tag{9}$$

L and e are the thicknesses of the B and A layers, respectively. This behavior was observed experimentally by Redon et al. for microscopic PDMS films on silanized silicon wafers.[11]

Experimental Section

Polystyrene and poly(methyl methacrylate) were chosen as model liquids for this study. At 162 °C, $S_{PS/PMMA} < 0$, so PS dewets PMMA. The interfacial energy between PMMA and silicon is smaller than the interfacial energy between PS and silicon, so PMMA was chosen as the lower layer. Monodisperse samples of both PS and PMMA are commercially available in a wide range of molecular weights. Samples were made with

Table 1. Characteristics of the Polymers Used in This Study

polymer	M_w	M_w/M_n	source	η (P)	thickness (Å)	η_{PS}/Θ_e
PS	65K	≤1.04	Pressure Chemical	2.1×10^4	270	1.2×10^5
PS	90K	≤1.04	Pressure Chemical	6.2×10^4	280	3.1×10^5
PS	200K	≤1.05	Pressure Chemical	9.3×10^5	280	6.5×10^6
PS	330K	≤1.04	Polymer Labs	5.2×10^4	280	2.6×10^7
PS	670K	≤1.06	Pressure Chemical	5.7×10^7	280	2.9×10^8
PMMA	27K	≤1.11	Polymer Labs	2.3×10^6	920	
PMMA	88K	≤1.11	Polymer Labs	1.3×10^8	850	
PMMA	330K	≤1.11	Polymer Labs	1.2×10^{10}	1000	

three different molecular weights of the PMMA lower layer, 27K, 88K, and 330K. For each of these, four different PS molecular weights were studied: 90K, 220K, 330K, and 670K. In addition, for the 330K PMMA lower layer, a 65K PS layer was made. The polydispersity of the polymers ranged between 1.04 and 1.11. Table 1 summarizes the characteristics of the polymers along with their viscosities at 162 °C.[12,13] The (equilibrium) contact angle for PS on PMMA has been measured previously with atomic force microscopy (AFM)[14] and was checked by examining a droplet in the late stage of dewetting (at 162 °C) and was found to be 10° as expected.

PMMA films (approximately 90 nm thick) were spin cast from a toluene solution onto silicon wafers and annealed at 160 °C in vacuum to remove any residual solvent. The thickness of the PMMA films was controlled by changing the concentration of the solution and was measured by ellipsometry. PS thin films (approximately 28 nm thick) were spin cast from a toluene solution onto microscope glass slides and floated off onto a bath of distilled water. These films were then carefully picked up on top of the PMMA films to form bilayers. Subsequently, the bilayers were annealed at 162 °C to initiate dewetting. The samples were removed from the oven and measured every 10−30 min depending on the dewetting velocity.

The dewetting velocity was determined by optical microscopy. An Olympus optical microscope was used to measure the diameter of the holes, which formed in the PS layer on annealing. The same area of the sample was investigated after each annealing step in order to follow the growth of individual holes. Figure 2 shows optical micrographs of the same area of a sample of 330K PS on 27K PMMA for three different annealing times. In addition to optical microscopy, some of the samples were investigated by AFM. A Digital Nanoscope III AFM with silicon nitride tips was operated in contact mode to examine the surface and interface morphology of the samples.

Results and Discussion

Figure 3 shows the diameter of holes in the PS film as a function of annealing time as determined from optical microscopy. Different PS molecular weights were studied for a 330K PMMA lower layer (Figure 3a), a 88K PMMA lower layer (Figure 3b), and a 27K PMMA lower layer (Figure 3c). The data points represent the mean values of at least 12 different holes, from which the statistical error is also calculated. The dewetting velocities span a range between 0.01 and 1 m/min.

Starting with Figure 3a, we see that the diameter of the holes grows linearly with time, indicating a constant dewetting velocity. The solid lines in the figure represent linear least-squares fits to the data. The lines are not necessarily expected to pass through the origin, since the holes have been formed either by capillary waves or by heterogeneities in the film, which lead to different initial conditions on the holes (i.e., $R \neq 0$ at $t = 0$). Since we observe the holes quite some time after they have formed, this is not important in determining the dewetting velocity. From Table 1, we note that, for the 330K PMMA lower layer, $\eta_{PMMA} > \eta_{PS}/\Theta_e$ for all PS molecular weights studied, so we expect the lower layer to be solidlike. Provided that $R(t) >> l(t)$, eq 4 should

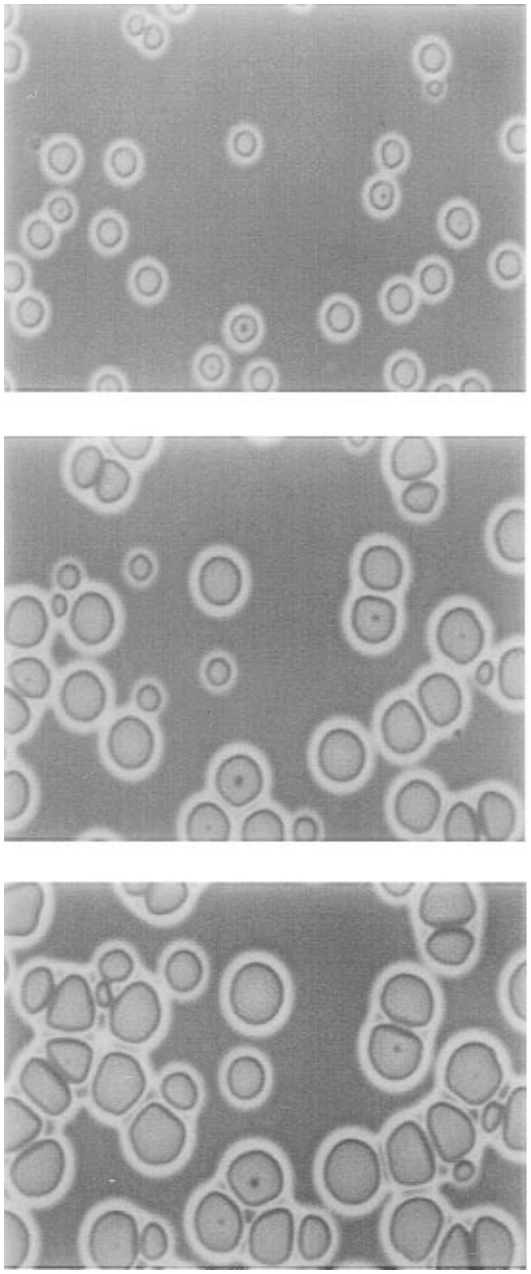

Figure 2. Optical micrographs showing holes in a sample of 330K PS on 27K PMMA after annealing for (a) 40, (b) 160, and (c) 280 min.

hold, and we expect a constant dewetting velocity, which is independent of the PMMA viscosity and which scales inversely with the PS viscosity. Before we test this prediction, we first verify eq 6 and show that, indeed, the width of the rim, $l(t)$, grows as the square root of time. To this end, we show AFM cross sections through the rim of a growing hole in a 90K PS film on the 330K PMMA lower layer for a range of hole diameters (Figure 4). To aid comparison, the cross sections are shifted

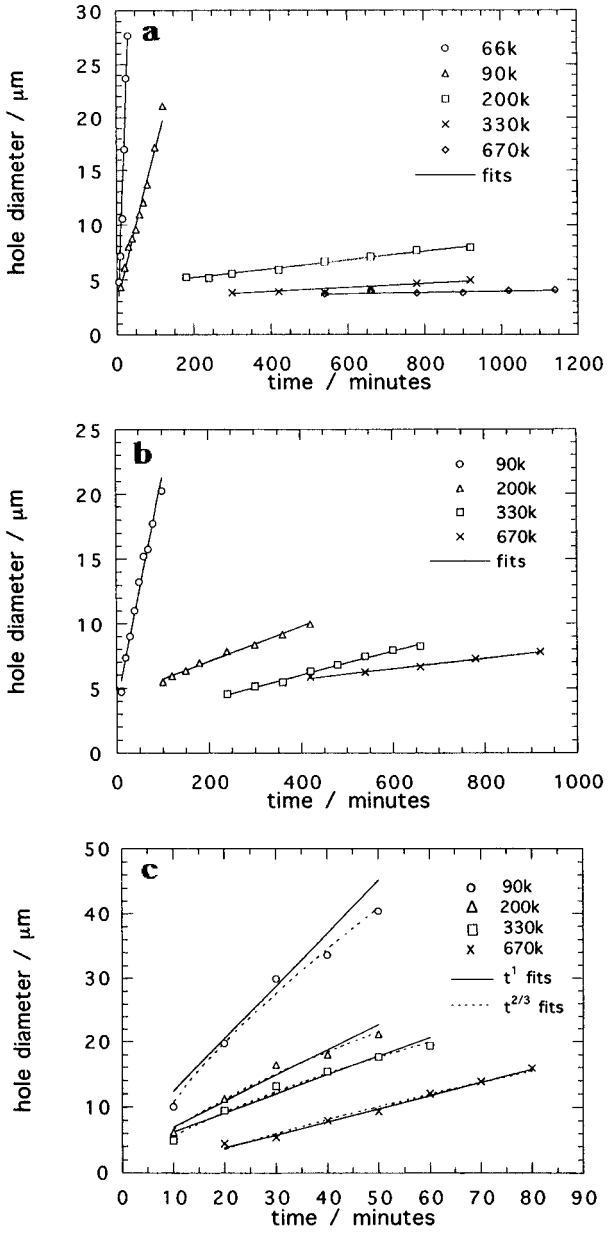

Figure 3. Hole diameter vs annealing time for (a) 330K PMMA, (b) 88K PMMA, and (c) 27K PMMA lower layer. In each case the 90K PS data are shown as circles, 200K PS, triangles, 330K PS, squares, and 670K PS, crosses. In part a only, the 65K PS data are shown as diamonds. In each case, the error bar is approximately the same size as the symbol. The solid lines are linear least-squares fits, and the dashed lines are fits with $v \propto t^{2/3}$.

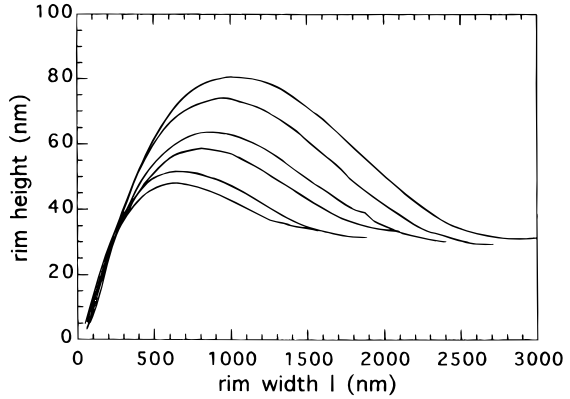

Figure 4. AFM cross sections through the rim of a hole in 90K PS on 330K PMMA for several hole diameters, shifted horizontally so that the inside edges of the rims are superposed.

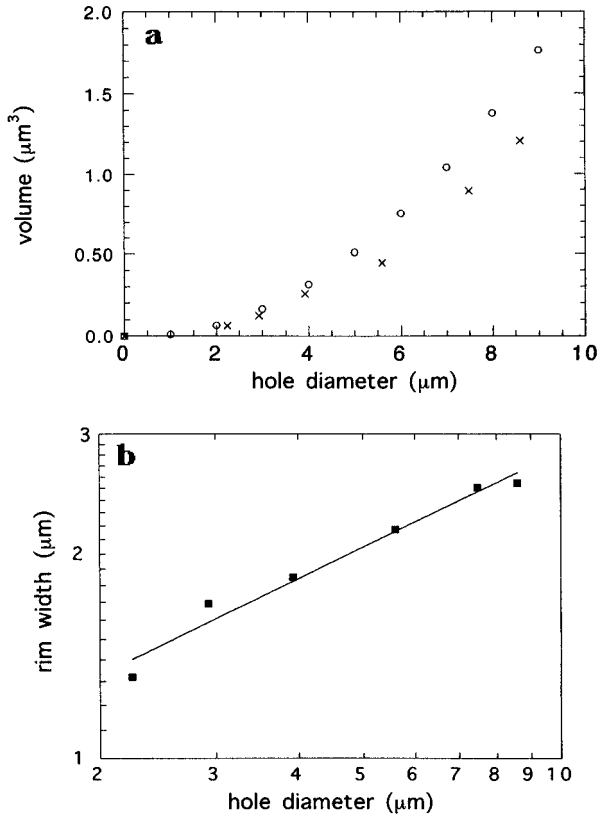

Figure 5. (a) Rim (crosses) and hole (circles) volumes as a function of the hole diameter. (b) log−log plot of the rim width against hole diameter.

horizontally so that the inside edges of the rims are superimposed. We can see that, as the hole grows, so does the rim. The widths of the rims (1 m) are smaller, though not very much smaller than the hole diameters (5 m). The (dynamic) contact angle remains constant at about 7.5, in good agreement with the prediction of eq 5. Figure 5a shows plots of the rim and hole volumes respectively as a function of the hole diameter. The volumes were obtained by integrating the AFM cross sections and assuming circular holes (the top of the PS layer away from the hole was taken as the baseline for the integration). As expected, the volumes increase in a similar manner, though the volume of the rim is somewhat smaller than that of the corresponding hole. This observation implies that some material can move from the rim into the bulk upper layer, i.e., that volume is not completely conserved between the rim and the hole. Figure 5b shows a plot of the rim width against the hole diameter from which we obtain $l(t)\ R^{0.48}$, in quantitative agreement with eq 6. Therefore the assumption $R >> l(t)$ made in the derivation of eq 4 seems to be valid.

For the 88K PMMA lower layer, $\eta_{PMMA} > \eta_{PS}/\Theta_e$ for all PS molecular weights except for the 670K PS. Again, we obtain good linear fits for all PS molecular weights studied; i.e., a constant dewetting velocity is observed for the 88K PMMA case too.

The viscosity of the 27K PMMA lower layer is less than that of the PS overlayers divided by the contact angle for all but the lowest PS molecular weight used (90K). Therefore, according to eq 7, the lower layer should behave as a liquid. Thus, there are two possibilities for the dewetting velocity (eqs 8 and 9) depending on whether or not the PMMA melt slips at

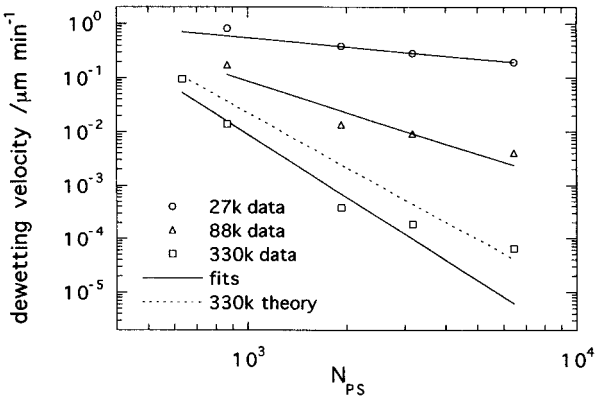

Figure 6. log−log plots of the dewetting velocity as a function of PS molecular weight: 27K PMMA lower layer (circles), 88K PMMA (triangles), and 330K PMMA (squares). The 330K data have been shifted vertically. The solid lines are linear least-squares fits which give $v \sim t^{-0.55}$ for 27K PMMA, $t^{-1.9}$ for 88K PMMA, and $t^{-3.9}$ for 330K PMMA. For the 330K the dashed line is the prediction of eq 5.

the substrate. We therefore expect that the hole size will grow linearly in time in the bulk lower layer regime, while a $t^{2/3}$ dependence is expected if slippage occurs (thin lower layer regime). Figure 3c shows the experimental data for the 27K PMMA lower layer. The error bars are approximately given by the size of the symbols. The results of least-squares fits assuming a linear behavior (solid lines) as well as a $t^{2/3}$ behavior (dashed lines) are shown together with the data. It is difficult to distinguish between the two fits. In the case of the 670K PS, a linear dependence fits the data better. For the 90K PS, on the other hand, the $t^{2/3}$ behavior results in the better fit. For the intermediate molecular weights, the data are consistent with both t dependencies. It is not possible to test the dependence of the dewetting velocity on parameters such as the PMMA molecular weight, the contact angle, or the interfacial tension with the present experiments, since we have only one data set with a liquidlike lower layer.

In Figure 6, the dewetting velocity is shown on a double-logarithmic plot as a function of the PS molecular weight for the 330K, 88K, and 27K PMMA lower layers. Linear least-squares fits were calculated by taking into account the estimated error bars and are shown as solid lines. For the calculation, only the data points satisfying $\eta_{PS} << \eta_{PMMA}$ were considered (i.e., 27K PMMA/90K PS and 88K PMMA/670K PS were omitted). We obtain good fits, from which the scaling of the velocity with PS molecular weight is determined ($v \sim N_{PS}^{\nu}$ where N_{PS} is the index of polymerization of PS). Figure 6 also shows the prediction of eq 5 for the solid lower layer (330K PMMA) as a dashed line using the known contact angle, viscosity, and surface tension for the PS. Although the theoretical line and the least-squares fit are somewhat different, the prediction is in reasonable agreement with the experimental data. For the solid lower layer (330K PMMA), we expect the dewetting velocity to scale as the inverse PS viscosity (eq 4), i.e., $v \sim N_{PS}^{-3.4}$.[13] This is consistent with the exponent of -3.9 ± 0.6 determined from the experimental data. For a liquid substrate, on the other hand, the dewetting velocity is expected to be independent of PS molecular weight. The experimental value found for the lowest PMMA molecular weight (27K PMMA lower layer) is small, but not zero (−0.55). For the 88K PMMA lower layers, an intermediate exponent of −1.9 is found, which is not predicted in any of the regimes described above.

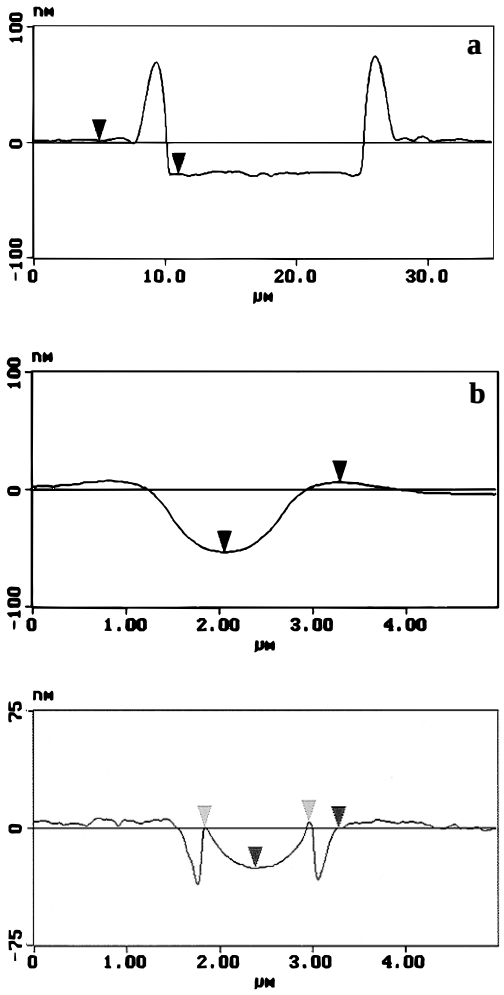

Figure 7. AFM cross section of droplets of (a) 90K PS on 330K PMMA annealed for 3 h (solid lower layer) and (b) 200K PS on 27K PMMA annealed for 3 h (liquid lower layer), both before and after washing in cyclohexane to remove the PS layer.

We shall return this finding below, after discussing the nature of the PS/PMMA interface.

Finally, we turn to the shape of the PS/PMMA interface in the vicinity of the rim for the different regimes discussed above. Lambooy et al. reported that the PS rim penetrates the PMMA layer in the liquid lower layer regime, whereas a flat PS/PMMA interface was observed in the solid substrate regime.[6] To check whether the lower layers in our samples are liquid- or solidlike, samples at an intermediate state of dewetting were examined by AFM. Images were taken before and after washing the samples in cyclohexane, which is a selective solvent for PS. If the lower layer is solidlike, we expect a featureless, flat film after removal of the PS (Young construction), whereas if the lower layer is liquidlike, we should see depressions in the PMMA lower layer under the PS rim (Neumann construction). Figure 7a shows an AFM cross section of a sample of 90K PS on 330K PMMA annealed for 3 h at 162 °C. The depth of the hole corresponds exactly to the known thickness of the top layer, and the hole has a flat bottom. After washing in cyclohexane, the sample appears flat and featureless. The observations confirm that the 330K PMMA layer is solid.

The 88K PMMA layer (not shown) has a depression under the rim similar to the observations of Lambooy et al.[6] Figure 7b shows AFM cross sections for a 200K PS on 27K PMMA. The unwashed sample exhibits a

rounded hole with a broad, shallow rim. The depth of the hole is about 55 nm, substantially greater than the thickness of the PS layer (28 nm). The volume of the hole is obviously much larger than the volume of the rim. These observations clearly show that there must be a rearrangement of material at the PS/PMMA interface, i.e., that the lower layer is liquidlike. The washed sample shows the structure of the PMMA layer beneath the hole and the rim. Again we observe a trench in the PMMA underneath the rim. However, here we observe also another interesting feature. The hole itself clearly extends into the PMMA layer, with the bottom lying 27 nm below the original PS/PMMA interface. A depression of the lower layer beneath the hole is not predicted by the theory of Brochard-Wyart et al.[1] Similar structures are observed for all PS molecular weights on the 27K PMMA lower layer. We speculate that it may be caused by strong shear forces, which arise as dewetting proceeds. This observation is being investigated further and will be reported in a forthcoming publication.[16]

We speculate that the intermediate exponent for the velocity as a function of molecular weight found for the 88K PMMA substrate may be related to the structure of the PS/PMMA interface. Very recent work by Brochard-Wyart and co-workers[15] shows that for a thin polymer film dewetting a solid substrate, if friction at the liquid/solid interface dominates, then the dewetting velocity is

$$v \propto \frac{|S|}{\eta_A}\sqrt{\frac{aN_A^{\,3}}{eN_B^{\,2}}} \sim N_A^{\,-1.9} \qquad (10)$$

where N_e is the entanglement degree of polymerization. It seems likely that the interfacial structure described above may be related to friction at the interface. Thus the two conditions of a solid lower layer and high friction may be satisfied in this case, and thus the dewetting velocity is given by eq 10. (Although the structure is also observed for the 27K sample, in that case the lower layer is liquid so the behavior is described by the C.b.1 regimes; the 330K shows no structure, so we infer low friction, and hence C.a.1 is valid.)

Conclusion

We have carried out a systematic and quantitative study of the dewetting of PS on PMMA as a function of molecular weight of both polymers. We have determined the scaling of the dewetting velocity with PS molecular weight and observed three regimes, as predicted by Brochard-Wyart et al.[1,15]

For high PMMA molecular weights (330K), the lower layer is solidlike and a constant dewetting velocity is found. The velocity scales with PS molecular weight as $N_{PS}^{-3.9\pm0.6}$. Both this scaling behavior and the absolute value of the dewetting velocity are in agreement with the theoretical prediction.[1] AFM images confirm the solid nature of the lower layer.

For low PMMA molecular weights (27K), the lower layer is liquidlike. The observed dewetting velocity is nearly independent of the upper layer molecular weight. It is mostly constant in time, though for some samples a $t^{2/3}$ behavior can not be excluded. AFM images confirm the liquid nature of the lower layer and show deep trenches in the lower layer underneath the rims. A deep depression was observed in the PMMA layer underneath the position of the holes.

For intermediate PMMA molecular weight (88K), the dewetting velocity is constant but scales as $N_{PS}^{-1.9\pm0.5}$ with the upper layer molecular weight. AFM images of the lower layer show a liquidlike substrate (depressions underneath the rims) but no depression underneath the holes. This exponent may be explained by friction at the PS/PMMA interface.

In summary, we have found quantitative agreement between our experiments and theoretical predictions for dewetting from solidlike and liquidlike substrate layers. We have shown that we can relate the dewetting velocity to the molecular weight of the upper layer when the lower layer is solid. It may therefore be possible to use dewetting to probe the viscosity of thin films. The structure of the liquid beneath the rim remains to be explained and will be discussed in greater detail in a forthcoming publication.

Acknowledgment. S.Q., M.H.R., and J.S. acknowledge financial support through grants from NSF (DMR9316157) and DOE (DE-SG02-93-ER45481), and C.J.C. acknowledges that from NSERC (CPG0163892). K.C.P. and G.K. are indebted to the Deutsche Forchungsgemeinschaft and to NATO (CRG No. 940599) for generous financial support. The authors thank F. Brochard-Wyart for helpful comments and for providing a preprint of ref 15.

References and Notes

(1) Brochard-Wyart, F.; Martin, P.; Redon, C. *Langmuir* **1993**, *9*, 3682.
(2) Reiter, G. *Phys. Rev. Lett.* **1992**, *68*, 75; *Langmuir* **1993**, *9*, 1944.
(3) Brochard-Wyart, F.; Daillant, J. *Can. J. Phys.* **1990**, *68*, 1084. Brochard-Wyart, F.; Redon, C.; Sykes, C. *C. R. Acad. Sci.* **1992**, *314*, 553.
(4) Jones, R. A. L. *Polymer* **1994**, *35*, 2160.
(5) Martin, P.; Buguin, A.; Brochard-Wyart, F. *Europhys. Lett.* **1994**, *28*, 421.
(6) Lambooy, P.; Phelan, K. C.; Haugg, O.; Krausch, G. *Phys. Rev. Lett.* **1996**, *76*, 1110.
(7) Young, T. *Philos. Trans. R. Soc. London* **1805**, *5*, 65.
(8) Tolan, M.; Li, Z.; Sokolov, J. Rafailovich, M. H., in preparation.
(9) Tanner, L. H. *J. Phys. D: Appl. Phys.* **1979**, *12*, 1473.
(10) Redon, C.; Brochard-Wyart, F.; Rondelez, F. *Phys. Rev. Lett.* **1991**, *66*, 715.
(11) Redon, C.; Brzoska, J. B.; Brochard-Wyart, F. *Macromolecules* **1994**, *27*, 468.
(12) Fox, T. G.; Flory, P. J. *J. Polym. Sci.* **1954**, *22*, 315.
(13) Doi, M.; Edwards, S. F. *The Theory of Polymer Dynamics*; Clarendon Press: Oxford, U.K., 1986.
(14) Israels, R.; Jasnow, D.; Balazs, A. C.; Guo, L.; Krausch, G.; Sokolov, J.; Rafailovich, M. H. *J. Chem. Phys.* **1995**, *102*, 8149.
(15) Brochard-Wyart, F.; Debregeas, G.; Fondecave, R.; Martin, P. *Macromolecules*, in press.
(16) Qu, S.; Clarke, C. J.; Rafailovich, M. H.; Sokolov, J., in preparation.

MA961297H